

First Principle Simulations of Heavy Fermion Cerium Compounds Based on the Kondo Lattice

Munehisa Matsumoto¹, Myung Joon Han¹, Junya Otsuki², and Sergey Y. Savrasov¹

¹ *Department of Physics, University of California, Davis, California 95616, USA and*

² *Department of Physics, Tohoku University, Sendai 980-8578, Japan*

(Dated: February 12, 2022)

We propose a new framework for first-principle calculations of heavy-fermion materials. These are described in terms of the Kondo lattice Hamiltonian with the parameters extracted from a realistic density functional based calculation which is then solved using continuous-time quantum Monte Carlo method and dynamical mean field theory. As an example, we show our results for the Néel temperatures of Cerium-122 compounds (CeX_2Si_2 with $X=\text{Ru, Rh, Pd, Cu, Ag, and Au}$) where the general trend around the magnetic quantum critical point is successfully reproduced. Our results are organized on a universal Doniach phase diagram in a semi-quantitative way.

PACS numbers: 71.27.+a, 75.20.Hr, 75.40.Mg

First-principle description of heavy-fermion materials has been a challenging problem for a long time. The difficulty arises from the dual nature of the electrons between localization and itinerancy due to the large Coulomb repulsion energy U at each site of the lattice. Here the relatively well-localized f -electrons interact with the itinerant s,p,d -electrons that form the conduction band. The heavy-fermion systems are generally described as the Anderson impurity model in the dilute limit [1] or the Anderson lattice model (ALM) in the dense limit, and the first-principle description of them has been done by several authors [2, 3, 4, 5]. With the development of dynamical mean field theory (DMFT) [6] and novel continuous-time quantum Monte Carlo (CT-QMC) solvers for the impurity problem [7, 8, 9], the ALM description has become quite successful except for a very low temperature range. The numerically exact treatment of the Anderson impurity problem is still very expensive if the temperature range of $O(1)$ K is to be reached. Thus, the first-principle description of strongly-correlated materials around the quantum critical point (QCP) [10], which has recently been attracting a lot of research interest is yet to be solved.

Here we attack the problem using the Kondo lattice model (KLM) trying to focus on the low-energy physics of the ALM. We show how this new approach works for a archetypical family of so called Cerium 122 compounds, CeX_2Si_2 ($X=\text{Ru, Rh, Pd, Cu, Ag, and Au}$), which has been one of the most extensively studied strongly-correlated materials since the discovery of heavy-fermion superconductor CeCu_2Si_2 [11]. Strictly speaking, we deal with the Coqblin-Schrieffer model [12] with full 14 fold degenerate f -shell but effectively the degeneracy is lowered due to the spin-orbit and crystal-field splittings. With the localized Kondo-impurity picture we can save the amount of the degrees of freedom in our model by eliminating charge fluctuations, and we can reach much lower temperature range as compared to the ALM simulations. The conduction band in the model is given by

the hybridization function between the localized $4f$ orbitals and the s,p,d -conduction bands calculated by the first-principle electronic structure calculation based on the local-density approximation (LDA) with Hubbard I [13] type of the self-energy for the f electrons. Then the Kondo coupling is defined via the Schrieffer-Wolff transformation [14], and the KLM is solved with the new efficient CT-QMC Kondo impurity solver [15] combined with DMFT.

Now we define the realistic KLM Hamiltonian for a given Cerium compound. The general Coqblin-Schrieffer Hamiltonian is the following.

$$\mathcal{H} = \sum_k \epsilon_k c_k^\dagger c_k + J_K \sum_{i\alpha\alpha'} f_{i\alpha}^\dagger f_{i\alpha'} c_{i\alpha'}^\dagger c_{i\alpha} + \sum_{i\alpha} \Delta_{\text{splitting}}^\alpha f_{i\alpha}^\dagger f_{i\alpha}, \quad (1)$$

Here ϵ_k is the conduction band, J_K is the Kondo coupling, $\Delta_{\text{splitting}}^\alpha$ is the crystal and spin-orbital field, c_k and $f_{i\alpha}$ are the annihilation operators for the conduction and $4f$ electrons, respectively, with the orbital α on the lattice site i . To solve this Hamiltonian we first need to define J_K and the conduction electron Green function. For this we perform the first principle DFT calculation within the local density approximation for s,p,d electrons plus the Hubbard I approximation for the f electrons based on the full-potential linearized muffin-tin orbitals (LMTO) method [13] and calculate the hybridization function [2] $\Im\Delta_\alpha(\epsilon) = \pi \sum_k |V_{\alpha k}|^2 \delta(\epsilon - \epsilon_k) \simeq \pi |V_\alpha|^2 \rho(\epsilon)$ where $V_{\alpha k}$ is the hybridization matrix element and $\rho(\epsilon)$ is the density of states of the conduction electrons at energy ϵ which we measure from the Fermi energy. We use experimental lattice parameters for all materials that we study.

The calculated $\text{Tr}\Im\Delta(\epsilon)/(\pi N_F) \equiv [1/(\pi N_F)] \sum_{\alpha=1}^{N_F} \Im\Delta_\alpha(\epsilon)$ is shown in Fig. 1 for several representative CeX_2Si_2 materials with $X=\text{Ru, Rh, Pd, and Ag}$. Here $N_F = 14$ is the total number of degeneracy and the trace of $\Im\Delta$ is taken over all of N_F states. We note that $\Im\Delta$ shows strong frequency dependence therefore in order to define J_K an averaging over some frequency intervals needs to be performed.

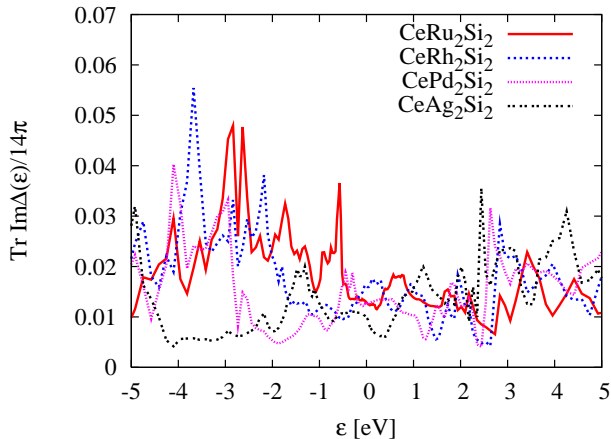


FIG. 1: (Color online) The hybridization function $\text{Tr}\Im\Delta(\epsilon)/14$ between the conduction band and the 4f-electrons calculated by LDA + Hubbard I for CeX_2Si_2 with $X=\text{Ru, Rh, Pd, and Ag}$. The origin of the energy is set to be the Fermi level.

The Kondo coupling J_K is defined by the Schrieffer–Wolff transformation [14, 16] as follows

$$J_K = \frac{1}{\pi} \int_{-D_{\text{cutoff}}}^{D_{\text{cutoff}}} d\epsilon \frac{\text{Tr}\Im\Delta(\epsilon)}{N_F} \left(\frac{1}{|\epsilon_f|} + \frac{1}{(\epsilon_f + U_{\text{eff}})} \right). \quad (2)$$

Here ϵ_f is the location of the energy level of 4f orbital, and $U_{\text{eff}} = U - J_{\text{Hund}}$ is the effective on-site Coulomb repulsion taking into account an effective Hund coupling J_{Hund} that works in the virtual f^2 state. We set $\epsilon_f = -2.5[\text{eV}]$ and $U = 5[\text{eV}]$ which is a typical value for Cerium compounds. The Hund coupling J_{Hund} is explored around a realistic value 1 eV as is explained below. In the present formulation, U_{eff} incorporates all of the possible multiplet effects in the virtual f^2 states and some systematic error comes in from the setting of this value, but it is small enough to see the general trend between the materials in the realistic Doniach phase diagram that is obtained in Fig. 4 in the end. Here we have a band cutoff D_{cutoff} set to be 5 [eV] which is large enough to make a universal description of the low-energy physics [17].

The portion of the conduction electron Green function $G_\alpha(\epsilon)$ which has non-zero hybridization with the f-electrons is also proportional to $\Delta_\alpha(\epsilon)$. We define the normalized and Hilbert-transformed $G_\alpha(i\omega)$ as follows

$$G_\alpha(i\omega) = \int_{-D_{\text{cutoff}}}^{D_{\text{cutoff}}} d\epsilon \frac{\Im\Delta_\alpha(\epsilon)}{i\omega - \epsilon} / \int_{-D_{\text{cutoff}}}^{D_{\text{cutoff}}} d\epsilon \Im\Delta_\alpha(\epsilon). \quad (3)$$

The Eqs. (2), (3) provide necessary inputs which are plugged into the CT-QMC and solved with DMFT self-consistency loop. The details of the CT-QMC algorithm for the Coqblin–Schrieffer model are given in [15]. These definitions for the realistic model are designed in such a way that it becomes exact in the limit of constant hy-

bridization with the relevant quantity $N_F J_K \rho(0)$ that determines the behavior of the KLM [15].

The LDA results for $N_F J_K \rho(0)$ for the target materials are given in Table I. The level splittings Δ_α appeared in 1 are implemented as the difference of the positions of ϵ_f 's which are used in the update probability as is described in Ref. [15]. These level splittings are taken from the literature and summarized in Table I. We checked that our results for the Néel temperatures are robust against small changes of factor of $O(1)$ on the level splittings. These Δ_α reduce the effective degeneracy close to $N_F = 2$ [18]. Thus we call our model “realistic Kondo” lattice instead of the Coqblin–Schrieffer lattice even though we are actually doing the multi-orbital model.

We apply the above framework for the KLM description of CeX_2Si_2 with $X=\text{Ru, Rh, Pd, Cu, Au, Ag}$. We do the following analyses with several settings of $U_{\text{eff}} = U - J_{\text{Hund}}$ for $0 \leq J_{\text{Hund}} \lesssim 1$ eV for each of the material. For a given material and given parameter set, we determine the Néel temperature by looking at the temperature dependence of staggered susceptibility and locating at which temperature it diverges. Here we follow the formalism of DMFT for the localized f-electron systems as given in [19] and use the same method as was utilized for model calculations in [20]. Regarding the realistic input of the Green's function as is depicted in Fig. 1, we make an approximation in the calculation of the staggered magnetic susceptibility for the 4f-electrons by decoupling the two-particle density of states $\rho(\epsilon_1, \epsilon_2) = \delta(\epsilon_1 + \epsilon_2)\rho(\epsilon_1)$ as if there is a nesting property which becomes exact when the 4f-electrons are on a hypercubic lattice. Thus the tendency to the antiferromagnetic order would be overestimated in addition to having the infinite-dimensional nature in the DMFT solution to the lattice problem. The data specific to CeRh_2Si_2 with which we determine the Néel temperatures for several settings of J_{Hund} are shown in Fig. 2. In this way for each of the material we look at the magnetic phase transitions for several J_K 's by varying corresponding J_{Hund} 's.

As was first discussed by Doniach [21, 22] and subsequently by many authors, Kondo lattices have two representative energy scales, namely the magnetic ordering energy that is proportional to $(J_K/N_F)^2 \rho(0)$ and the Kondo screening energy which behaves like $\exp(-1/N_F J_K \rho(0))$. For small J_K 's the former wins but as J_K becomes larger the exponential growth of the latter dominates at some point. Thus a given system can realize in either magnetically ordered phase or non-magnetic Kondo-screened phase. Between these two phases at zero temperature there is thought to be a QCP. We explore this Doniach phase diagram for each material and find the material-specific QCP. We take the data with the setting $J_{\text{Hund}} = 0.94$ eV as our realistic result for each material as this strength of the Hund coupling is close to the realistic value and also gives reasonable trend over all materials in the family. Thus obtained Doniach phase diagrams for

TABLE I: Inputs (given by LDA and experiments in the literature) and outputs for each material. $\Delta_{\text{spin-orbit}}$ is spin-orbit splitting between $j = 5/2$ and $j = 7/2$ states. Crystal field splitting of $j = 5/2$ state produces three doublets with energy $E_0 < E_1 < E_2$ with $E_1 - E_0 = \Delta_{\text{splitting}}^1$ and $E_2 - E_0 = \Delta_{\text{splitting}}^2$. $J_{\text{Hund}} \sim 1$ eV is used. The $\Delta_{\text{splitting}}^1$, $\Delta_{\text{splitting}}^2$, $\Delta_{\text{splitting}}^{\text{spin-orbit}}$ are given in meV unit and T_N in K. Similar values for the level splittings were used in a recent work [37].

material	$N_F J_K \rho(0)$	$\Delta_{\text{splitting}}^1$	$\Delta_{\text{splitting}}^2$	$\Delta_{\text{splitting}}^{\text{spin-orbit}}$	T_N (literature)	T_N (our results)
CeRu ₂ Si ₂	0.144	19 ^{a,b}	34 ^{a,b}	~ 300	(paramagnetic) ^h	0
CeRh ₂ Si ₂	0.180	26.7 ^c	58.7 ^c	~ 300	36–39 ^h	~ 70
CePd ₂ Si ₂	0.140	19 ^{d,e}	24 ^{d,e}	230 ^d	10 ^h	~ 50
CeCu ₂ Si ₂	0.146	32 ^{b,J,g}	37 ^{b,J,g}	~ 300	(paramagnetic) ^h	~ 70
CeAg ₂ Si ₂	0.110	8.8 ^e	18.0 ^e	~ 300	8–10 ^h	~ 30
CeAu ₂ Si ₂	0.125	16.5 ^e	20.9 ^e	~ 300	8–10 ^h	~ 50

^a Ref. [29] ^b Ref. [30] ^c Ref. [31] ^d Ref. [32] ^e Ref. [33] ^f Ref. [34] ^g Ref. [35] ^h Ref. [36]

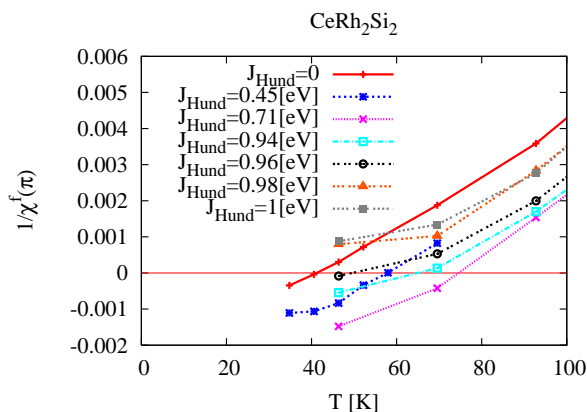


FIG. 2: (Color online) Determination of Néel temperatures for several settings of the Hund coupling J_{Hund} . We see that the Néel temperature disappears at the point where J_{Hund} takes the value between 0.96 and 0.98 eV.

all of the materials are shown in Fig. 3.

Now we can plot all of the six materials CeX_2Si_2 ($X=\text{Ru,Rh,Pd,Cu,Ag,Au}$) on the universal Doniach phase diagram in the same spirit as was done by Endstra et al. in 1993 [36] but with a different horizontal axis. In the material-specific Doniach phase diagrams in Fig. 3, we see that the locations of QCP's on the $N_F J_K \rho(0)$ are not actually universal [23]. So we measure the distance between the QCP and the material's realistic location on the horizontal axis, $N_F J_K \rho(0) - N_F J_K \rho(0)|_{\text{QCP}}$, and plot the Néel temperatures with respect to the value of the distance to QCP defined as $t \equiv [N_F J_K \rho(0) - N_F J_K \rho(0)|_{\text{QCP}}] / N_F J_K \rho(0)|_{\text{QCP}}$. The result is shown in Fig. 4. We expect a systematic error bar in the estimation of the value on the horizontal axis especially around the QCP but these possible systematic errors are small enough to discern the locations of CeX_2Si_2 ($X=\text{Ag,Au}$) and CeRh_2Si_2 . The antiferromagnet CeRh_2Si_2 and the paramagnet CeCu_2Si_2 are mixed up within the present level of resolution which is manifested by the result that finite Néel temperature is plotted for CeCu_2Si_2 . However, this is actually caused by the proximity of this ma-

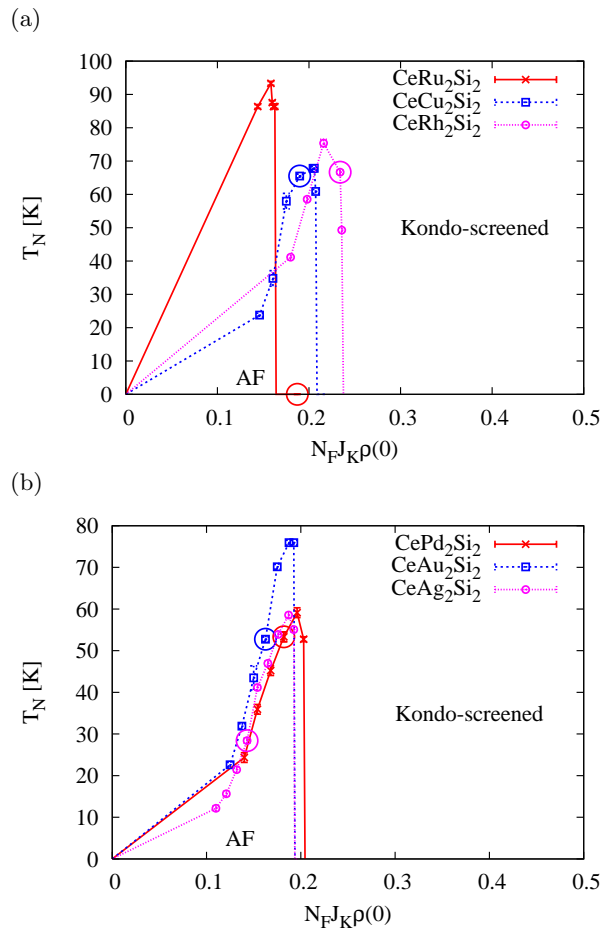


FIG. 3: (Color online) Material specific Doniach phase diagrams for CeX_2Si_2 with (a) $X=\text{Ru,Cu, and Rh}$ and with (b) $X=\text{Pd, Au, and Ag}$. The realistic results with $J_{\text{Hund}} = 0.94$ eV are marked with the larger plot symbols.

terial to its QCP as can be seen from Fig. 3. So our numerical result is consistent with the experimental result that CeCu_2Si_2 is a superconductor at ambient pressure and is thought to be close to the QCP.

We note that the valence fluctuations which we ignored in our simulation could be important in the realization of

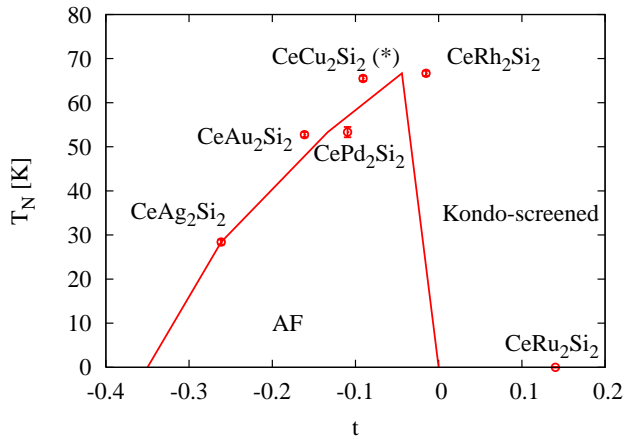


FIG. 4: (Color online) Universal Doniach phase diagram for the material family of CeX_2Si_2 . The horizontal axis is defined as follows: $t \equiv [N_F J_K \rho(0) - N_F J_K \rho(0)|_{\text{QCP}}] / N_F J_K \rho(0)|_{\text{QCP}}$. The line is guide for the eye. We plot CeCu_2Si_2 with an asterisk mark to note as it apparently has a finite Néel temperature but that just reflects the result that CeCu_2Si_2 is very close to QCP as can be seen in Fig. 3.

the non-magnetic ground state. Indeed it is known that there are some valence fluctuations in CeCu_2Si_2 [24] and CeRu_2Si_2 [25]. This might make the possible systematic error relatively larger on the right-hand side of our phase diagram [26, 27]. Nevertheless at the present level of description we believe that the realistic KLM works because the number of 4f electrons in Cerium ion is still very close to one [24, 25]. At least for the impurity problem the convergence to the Kondo impurity picture in large $|\epsilon_f|/(\rho(0)V^2)$ limit of the Anderson model was discussed exactly [28]. Careful comparison between the Anderson lattice and the Kondo lattice regarding the valence fluctuation issue is interesting, especially for CeCu_2Si_2 , and further work is ongoing in this direction.

MM thanks Y.-F. Yang, P. Werner, and H. Shishido for helpful discussions and N. Matsumoto for continuous supports. Discussions with the participants in ICAM-DCHEM workshop in August 2008 are acknowledged. This research is supported by NSF Grant No. DMR-0606498 and by DOE SciDAC Grant No. SE-FC02-06ER25793. Numerical computations are performed using TeraGrid supercomputer grant No. 090064.

[1] P. W. Anderson, Phys. Rev. **124**, 41 (1961).
 [2] J. E. Han, M. Alouani, and D.L. Cox, Phys. Rev. Lett. **78**, 939 (1997).
 [3] M. B. Zöfl, I. A. Nekrasov, Th. Pruschke, V. I. Anisimov, and J. Keller, Phys. Rev. Lett. **87**, 276403 (2001).
 [4] K. Held, A. K. McMahan, and R. T. Scalettar, Phys. Rev. Lett. **87**, 276404 (2001).
 [5] J. H. Shim, K. Haule, G. Kotliar, Science **318**, 1615

(2007).
 [6] A. Georges *et al.* Rev. Mod. Phys. **68**, 13 (1996).
 [7] A. N. Rubtsov, V. V. Savkin, and A. I. Lichtenstein, Phys. Rev. B **72**, 035122 (2005).
 [8] P. Werner, A. Comanac, L. de' Medici, M. Troyer, and A. Millis, Phys. Rev. Lett. **97**, 076405 (2006); P. Werner and A. Millis, Phys. Rev. B **74**, 155107 (2006).
 [9] K. Haule, Phys. Rev. B **75**, 155113 (2007).
 [10] S. Sachdev, *Quantum Phase Transitions*, Cambridge (1999).
 [11] F. Steglich *et al.*, Phys. Rev. Lett. **43**, 1892 (1979).
 [12] B. Coqblin and J. R. Schrieffer, Phys. Rev. **185**, 847 (1969).
 [13] For a review, G. Kotliar *et al.* Rev. Mod. Phys. **78**, 865 (2006).
 [14] J. R. Schrieffer and P. A. Wolff, Phys. Rev. **149**, 491 (1966).
 [15] J. Otsuki, H. Kusunose, P. Werner and Y. Kuramoto, J. Phys. Soc. Jpn. **76**, 114707 (2007).
 [16] B. Mühlischlegel, Z. Phys. **208**, 94 (1968).
 [17] The definition of J_K should always be combined with the cutoff scheme for the conduction band as is discussed in N. Andrei *et al.*, Rev. Mod. Phys. **55**, 331 (1983).
 [18] For isotropic $N_F = 14$ KLM the Néel temperature is vanishing small while for $N_F = 2$ the Néel temperature looks unrealistically large [20]. We can observe realistic Néel temperatures when realistic level splittings are introduced.
 [19] J. Otsuki, H. Kusunose, and Y. Kuramoto, J. Phys. Soc. Jpn. **78**, 014702 (2009)
 [20] J. Otsuki, H. Kusunose, and Y. Kuramoto, J. Phys. Soc. Jpn. **78**, 034719 (2009).
 [21] S. Doniach, Physica B **91**, 231 (1977).
 [22] S. Doniach, Phys. Rev. B **35**, 1814 (1987).
 [23] Recent update of Doniach phase diagram also discussed this point: Y.-f. Yang *et al.*, Nature **454**, 611 (2008). Also the sensitiveness of the quantum critical point to the system-specific features was discussed in V. Yu. Irkhin and M. I. Katsnelson, Phys. Rev. B **56**, 8109 (1997).
 [24] P. H. Ansari *et al.*, J. Appl. Phys. **63**, 3503 (1987).
 [25] M. Yano *et al.*, Phys. Rev. B **77**, 035118 (2008).
 [26] The importance of valence fluctuations in CeCu_2Si_2 has been discussed in the following paper: A. H. Holmes, D. Jaccard, and K. Miyake, Phys. Rev. B **69**, 024508 (2004).
 [27] However both of the Anderson lattice and the Kondo lattice have the large Fermi surface, see, e.g. J. Otsuki, H. Kusunose, and Y. Kuramoto, Phys. Rev. Lett. **102**, 017202 (2009), and references therein.
 [28] P. Schlottmann, Z. Phys. B **57**, 23 (1984).
 [29] G. Zwicknagl, Adv. Phys. **41**, 203 (1992).
 [30] D. Ehm *et al.* Phys. Rev. B **76**, 045117 (2007).
 [31] R. Settai *et al.* J. Phys. Soc. Jpn. **66**, 2260 (1997).
 [32] P. Hansmann *et al.* Phys. Rev. Lett. **100**, 066405 (2008).
 [33] A. Severing *et al.* Phys. Rev. B **39**, 2557 (1989).
 [34] E. A. Goremychkin and R. Osborn, Phys. Rev. B **47**, 14280, (1993).
 [35] We note that a crystal-field splitting scheme for CeCu_2Si_2 mentioned in [33] is obsolete.
 [36] T. Endstra, G. J. Nieuwenhuys, and J. A. Mydosh, Phys. Rev. B **48**, 9595 (1993).
 [37] V. Vildosola *et al.* Phys. Rev. B **71**, 184420 (2005).